Chemical Physics Letters 486 (2010) 104–109

Contents lists available at ScienceDirect

Chemical Physics Letters

journal homepage: www.elsevier.com/locate/cplett

Theoretical studies of ZEKE spectroscopy and dynamics of high Rydberg states

Yi-Hsieh Wang [a,e], Y. Teranishi [b,c], H. Mineo [a], S.D. Chao [a,*], H.L. Selzle [d], H.J. Neusser [d], E.W. Schlag [d], S.H. Lin [b,c,e]

[a] Institute of Applied Mechanics, National Taiwan University, Taipei 106, Taiwan
[b] Institute of Atomic and Molecular Sciences, Academia Sinica, Taipei 106, Taiwan
[c] Institute of Applied Chemistry, Institute of Molecular Science, Chiao-Tung University, Hsin-Chu, Taiwan
[d] Institut für Physikalische und Theoretische Chemie, Technische Universität München, Lichtenbergstr. 4, D-85748 Garching, Germany
[e] Research Center for Applied Sciences, Academia Sinica, Taipei 115, Taiwan

ARTICLE INFO

Article history:
Received 22 September 2009
In final form 29 December 2009
Available online 11 January 2010

ABSTRACT

A main purpose of this Letter is to show how to employ the inverse Born–Oppenheimer approximation as a basis set to study zero kinetic energy (ZEKE) spectroscopy and the autoionization dynamics of the ZEKE states. The calculations of channel couplings, quantum defects, intensity borrowing, vibrational and rotational autotionizations will be demonstrated by using a homonuclear diatomic molecule as an example.

1. Introduction

Since its invention by Müller–Dethlefs, Sander and Schlag in 1984 [1,2], the zero kinetic energy (ZEKE) spectroscopy has seen the explosive activity in high resolution spectroscopy of the ions. Using this technique, the first examples of full rotational resolution in photoelectron spectra (PES) have been obtained. Consequently, there has been a considerable impetus given to the understanding of the behavior of molecules very close to their ionization thresholds.

However, while the power of the ZEKE technique to determine ionization potential (IP) of molecules and ionic rovibronic energies with high accuracy is widely recognized, and has been illustrated in many systems, the interpretation of rotational line intensities and dynamics of ZEKE states still poses some problems [3,4]. For example, do the ZEKE line intensities reflect direct ionization cross-sections? Are ZEKE-PES intensities consistent with conventional PES intensities? Can they be predicted by ab initio calculations? Is there a systematic procedure to extract meaningful information from ZEKE line intensities? Rotational and vibrational autoionizations are believed to play important roles in ZEKE spectroscopy. How can they be evaluated credibly? Anomalous intense peaks are often observed in ZEKE spectroscopy and they are usually attributed to some resonance effects. How can we treat these resonance phenomena? In this Letter, we shall attempt to answer these questions by employing the theory of ZEKE spectroscopy based on the use of inverse Born–Oppenheimer approximation (IBOA) [5–8].

For simplicity of demonstration, we shall use a homonuclear diatomic molecule as an example to demonstrate how to calculate channel couplings, quantum defects, intensity borrowing in ZEKE spectroscopy, and dynamics of rotational and vibrational autoionization. In our opinion, the observed ZEKE band-shapes should depend on optical pumping of ZEKE levels, l mixing induced by a stray field, field-induced lowering of ionization thresholds, electric field-induced ionization, tunneling ionization, and autoionization. The ZEKE band-shapes will not be studied in this Letter, but will be reported in a future paper.

The present Letter will be organized as follows. In Section 2, a typical ZEKE spectroscopy experiment will be presented and the IBOA will be described. In Sections 3–5, we shall show how to use the IBOA to study quantum defects, and rotational and vibrational autoionizations, respectively. These will be followed by discussion which is presented in Section 6.

2. General consideration

In treating ZEKE spectroscopy and dynamics of the ZEKE Rydberg states, the multi-channel quantum defect theory (MQDT) is commonly used [3,4,9–11], which is combined with the photo-electron spectroscopy model [12–17]. In this Letter, we shall use the inverse Born–Oppenheimer approximation (IBOA) to study these phenomena. Some preliminary results have been reported [5–7]. Several types of ZEKE experiments have been proposed [1–4]. For convenience of discussion, one of these experiments will be briefly described, which is based on the one-photon absorption [5,6], and shown in Fig. 1.

Consider a photoexcitation from state $K(a\upsilon)$ to state $M(cwm)$, where a and c denote electronic states and υ and w denote

* Corresponding author. Fax: +886 2 2363 9290.
E-mail address: sdchao@iam.ntu.edu.tw (S.D. Chao).

0009-2614/$ - see front matter © 2010 Elsevier B.V. All rights reserved.
doi:10.1016/j.cplett.2009.12.092

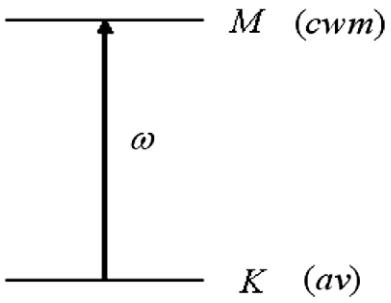

Fig. 1. A schematic plot showing a one-photon ZEKE spectroscopy. The transition by a laser of frequency ω is from state $K(av)$ to state $M(cwm)$. See text for more details.

rovibrational states, and m denotes the Rydberg electron state. In the dipole approximation, the interaction Hamiltonian is

$$\hat{H}' = -\vec{\mu}\cdot\vec{E}_0\cos\omega t \tag{2.1}$$

where $\vec{\mu}$ is the dipole moment, $\vec{E}_0$ and ω are the electric field and frequency of the laser field, respectively, and the absorption rate constant $W^{(1)}_{K\to M}$ is given by

$$W^{(1)}_{K\to M} = \frac{\pi}{2\hbar^2}|\vec{\mu}_{MK}\cdot\vec{E}_0|^2 D(\omega_{MK}-\omega) \tag{2.2}$$

where $\vec{\mu}_{MK}$ denotes the transition dipole moment and $D(\omega_{MK}-\omega)$ represents the line-shape function. The latter can be Lorentzian or Fano-type of line-shape depending on whether the M-level is isolated or coupled to a continuum. The thermal average rate constant $W^{(1)}$ is given by

$$\begin{aligned} W^{(1)} &= \sum_K\sum_M P_K W^{(1)}_{K\to M} \\ &= \frac{\pi}{2\hbar^2}\sum_K\sum_M P_K|\vec{\mu}_{MK}\cdot\vec{E}_0|^2 D(\omega_{MK}-\omega) \end{aligned} \tag{2.3}$$

where P_K denotes the Boltzmann distribution.

It should be noted that the absorption rate constants given by Eqs. (2.2) and (2.3) can easily be converted into the corresponding absorption coefficients or cross sections. However, the measurements of ZEKE signals involve not only the optical absorption from the transition of, for example, $(av)\to(cwm)$ but also the extraction of ZEKE electrons from ZEKE states (cwm) by a discriminating field and an extraction field. This is the reason why the absorption rate constants, instead of the absorption coefficients, are being used in treating ZEKE spectroscopy in this Letter.

In this Letter, we shall choose the inverse Born–Oppenheimer approximation [5–7] as a basis set for the ZEKE experiment. The molecular Hamiltonian in this case can be expressed as

$$\hat{H} = \hat{H}_{ion} + \hat{T}_e \tag{2.4}$$

where $\hat{H}_{ion}$ is the Hamiltonian of the ion and $\hat{T}_e$ denotes the kinetic energy operator of the ZEKE electron. It follows that

$$\hat{H}\Psi_{cwm} = E_{cwm}\Psi_{cwm} \tag{2.5}$$

$$\Psi_{cwm} = \Phi_{cwm}\Theta_{cw} \tag{2.6}$$

$$\hat{H}_{ion}\Theta_{cw} = U_{cw}\Theta_{cw} \tag{2.7}$$

and

$$(\hat{T}_e + U_{cw})\Phi_{cwm} = E_{cwm}\Phi_{cwm} \tag{2.8}$$

This shows that the ZEKE electron is moving in the potential energy surface provided by the ion core described by (cw). The energy levels within IBOA are shown graphically in Fig. 2. In the figure, ZEKE states (cwm) below the rovibronic state (cw) of the ion are discrete while those above (cw) are continuous (cwk). Here we refer to the high Rydberg states near but below the ionization continuum as 'ZEKE Rydberg' states.

Based on the IBOA model for ZEKE spectroscopy, the ab initio calculations can be applied to calculate transition dipole moments involved in absorption rate constants shown in Eqs. (2.1)–(2.3). It should be noted that nearly all ZEKE experiments involve pulse-field ionization of very high Rydberg states just below threshold, rather than extraction of true ZEKE electrons at, or above threshold. The Rydberg states form a pseudo-continuum, and as a consequence of the continuity of the transition probability on either side of an ionization limit, it is often assumed that the ZEKE transition intensities can be treated in the same manner as true photoionization intensities [12–17].

It should be noted that in the BOA model, the kinetic energy operator of nuclear motion $\hat{T}_n$ can be used to treat the excited state dynamics like internal conversion [18] and autoionization of low Rydberg states [19]. In a similar manner, the kinetic energy operator of the ZEKE electron $\hat{T}_e$ can be employed to treat rotational and vibrational autoionization, as will be shown below.

Based on the use of the IBOA, the model of the ZEKE spectroscopy and the dynamics of its Rydberg states can be shown in Fig. 2. Here the Born–Oppenheimer approximation (BOA) is used to describe the neutral molecule. From this figure we can see that the ZEKE spectroscopy is related to the transition from the rovibronic state of the neutral molecule (av) or Ψ_{av}. In the BOA, $\Psi_{av} = \Phi_a\Theta_{av}$ where Φ_a and Θ_{av} represent the wavefunctions of the electronic motion and nuclear motion, respectively. We can also see that in the IBOA, the channel coupling is due to the coupling between (cwm) and $(cw'm')$ while the autoionization is due to the coupling of the ZEKE states (cwm) with the ZEKE continuum states $(cw'k')$.

3. Quantum defect

Due to the channel couplings, each ZEKE state is not pure and thus we can calculate the quantum defect for a ZEKE state and the intensity borrowing in the ZEKE spectroscopy. For example, we can calculate the quantum defect as follows. Suppose that we let n denote the ZEKE state (cwm) under consideration which will be coupled to other lower Rydberg states like $n_1, n_2, \ldots$ by the channel couplings as shown in Fig. 2. Then we have

$$\Psi_n = C_{n,n}\Psi^0_n + C_{n,n_1}\Psi^0_{n_1} + C_{n,n_2}\Psi^0_{n_2} + \cdots \tag{3.1}$$

and

$$\hat{H}\Psi_n = E_n\Psi_n \tag{3.2}$$

$$C_{n,n}(H_{n,n}-E) + C_{n,n_1}H_{n,n_1} + C_{n,n_2}H_{n,n_2} + \cdots = 0 \tag{3.3}$$

$$C_{n_1,n}H_{n_1,n} + C_{n_1,n_1}(H_{n_1,n_1}-E) = 0 \tag{3.4}$$

$$C_{n_2,n}H_{n_2,n} + C_{n_2,n_2}(H_{n_2,n_2}-E) = 0 \tag{3.5}$$

$$\cdots$$

Here we assume that the couplings like H_{n_i,n_j} $(i\neq j)$ can be neglected. It follows that

$$E = H_{n,n} + \sum_{n_i}\frac{|H_{n,n_i}|^2}{E-H_{n_i,n_i}} \tag{3.6}$$

or approximately

$$E = H_{n,n} + \sum_{n_i}\frac{|H_{n,n_i}|^2}{H_{n,n}-H_{n_i,n_i}} \tag{3.7}$$

In this Letter, for demonstration we shall consider the applications of the IBOA model to the dynamics and spectroscopy of ZEKE states of homonuclear diatomic molecules. In the following we consider a simple model. Notice that U_{cw} in the Schrödinger equation of the

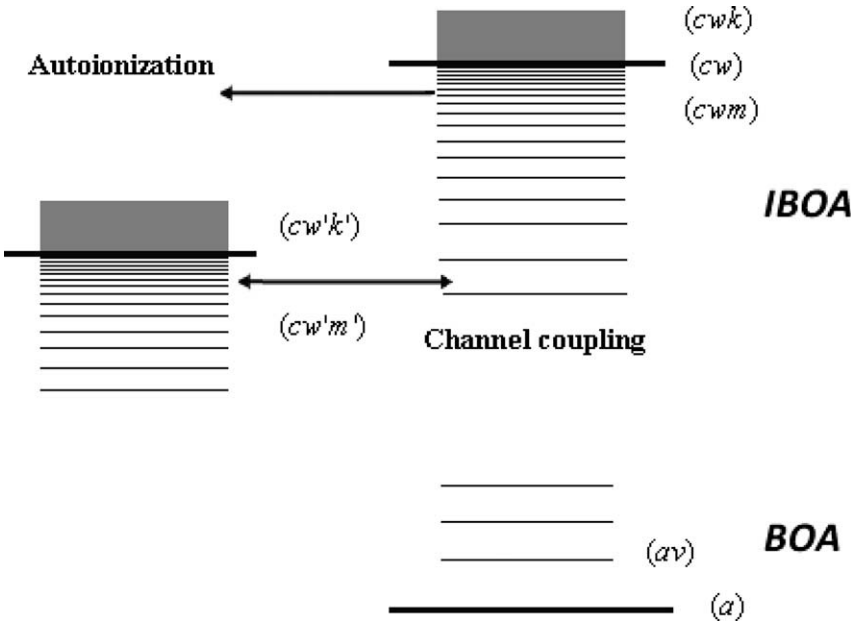

Fig. 2. A schematic plot showing the channel coupling $(cwm) \leftrightarrow (cw'm')$ and the autoionization $(cwm) \leftrightarrow (cw'k)$ mechanisms.

molecular ion core, Eq. (2.7), consists of the rovibronic energy levels E_{cw} of the molecular ion plus the potential energy V_e of the ZEKE electron. That is,

$$(\hat{T}_e + V_e)\Phi_{cwm} = \varepsilon_{cwm}\Phi_{cwm} \tag{3.8}$$

where

$$\varepsilon_{cwm} = E_{cwm} - E_{cw}; \quad V_e = U_{cw} - E_{cw} \tag{3.9}$$

For V_e we shall for simplicity use the multipole expansion

$$V_e = -\frac{e^2}{r} + V'_q \tag{3.10}$$

$$V'_q = -e\frac{Q(R)}{r^3}\left[\frac{4\pi}{5}\sum_{\bar{m}=-2}^{2} Y_{2\bar{m}}(\theta,\phi)Y^*_{2\bar{m}}(\Theta,\Phi)\right] \tag{3.11}$$

where $Q(R)$ denotes the core quadrupole moment.

For our purpose, we shall use the notations; v^+ and N^+ denote the vibrational and rotational quantum numbers of the ion, while (nlm) represents the quantum numbers of high Rydberg states.

The quantum defect of N_2 has been experimentally determined by Merkt and Softley [10,20–22]. In the following, we demonstrate how to calculate it by choosing the state $\{v^+ = 0,\ N^+ = 0(nlm)\}$ as an example. Notice that

$$\begin{aligned}\left\langle v'^+ = 0,\ N'^+ = 2(n'l')\middle|V'_q\middle|v^+ = 0,\ N^+ = 0(nl)\right\rangle \\ = -e\langle\chi_{v'^+=0}|Q(R)|\chi_{v^+=0}\rangle\langle R_{n'l'}|r^{-3}|R_{nl}\rangle \\ \times\left[\frac{4\pi}{5}\sum_{mM^+}\sum_{m'M'^+}\sum_{\bar{m}}\langle Y_{l'm'}|Y_{2\bar{m}}|Y_{lm}\rangle\left\langle Y_{N'^+=2,M'^+}\middle|Y^*_{2\bar{m}}\middle|Y_{N^+=0,M^+}\right\rangle\right]\end{aligned} \tag{3.12}$$

and

$$\begin{aligned}\langle R_{n',l'}|r^{-p}|R_{n,l}\rangle = [(n+l)!(n-l-1)!]^{\frac{1}{2}}[(n'+l')!(n'-l'-1)!]^{\frac{1}{2}} \\ \times\sum_{\lambda=0}^{n-l-1}\sum_{\lambda'=0}^{n'-l'-1}\left[(-1)^{\lambda+\lambda'}2^{l+l'+\lambda+\lambda'+2}\frac{(l+l'+\lambda+\lambda'-p+2)!}{(n^{-1}+n'^{-1})^{l+l'+\lambda+\lambda'-p+3}}\right. \\ \left.\times F(nl,\lambda)F(n'l',\lambda')\right]\end{aligned} \tag{3.13}$$

where

$$F(nl,\lambda) = (n^{-1})^{l+\lambda+2}(\lambda!)^{-1}[(n-l-1-\lambda)!]^{-1}[(2l+1-\lambda)!]^{-1} \tag{3.14}$$

and a similar expression for $F(n'l',\lambda')$.

Therefore, we can calculate the quantum defect as the energy correction in Eq. (3.7) and evaluate the matrix element by Eq. (3.12). Our preliminary results show that there seems no definite correlation between the quantum defects and the rotational quantum number. For example, for $n = 200$ we obtain the quantum defects of −0.158, −0.322, 0.825 for $N^+ = 1, 2, 3$, respectively. On the other hand from the formulation shown in the above, it is clear the vibrational quantum number dependence of the quantum defect is roughly linear. This has been found to be consistent with the experimental observation [7].

Merkt and Softley reported the rotationally resolved ZEKE spectra of N_2 for the bands $X^2\Sigma_g^+(v^+ = 0, 1) \leftarrow X'\Sigma_g^+(v = 0)$ [10]. For $(v^+ = 0) \leftarrow (v = 0)$ band, they observed that the Q-branch is strong and the O-branch is weak, and pointed out that the intensity borrowing takes place. This intensity borrowing can be treated by calculating the corresponding matrix elements similar to Eq. (3.12). Our calculations show that the transition $0' \to 2^+$ of the S-branch, due to the channel coupling, can borrow the $0' \to 0^+$ of the Q-branch, due to the large gap $E_{2^+} - E_{0^+}$ (that is, off-resonance), the $0' \to 2^+$ transition is weak as experimentally observed. The O-branch $2' \to 0^+$ can borrow the intensity from $2' \to 2^+$. For the $(v' = 0 \to v^+ = 0)$ of N_2, the spectral intensities of various bands of S, O, M, ... branches are determined by the intensity borrowing from the Q-band and are determined by the energy differences like $E_{4^+} - E_{0^+}$, $E_{0^+} - E_{2^+}$, etc. For O-branch, M-branch, etc., accidental resonances can happen to these energy gaps and consequently, some anomalous peaks can be observed.

4. Rotational autoionization

We start with the Fermi golden rule expression for rotational autoionization using the IBOA as a basis set [5–7]

$$W_{(cwm\to cw'k)} = \frac{2\pi}{\hbar}\left|\left\langle\Psi_{cw'k}\middle|\hat{H}'_{IBO}\middle|\Psi_{cwm}\right\rangle\right|^2\rho(E_k) \tag{4.1}$$

where $\rho(E_k)$ is the density of state around energy E_k. Notice that

$$\left\langle \Psi_{cw'k}\middle|\widehat{H}'_{IBO}\middle|\Psi_{cwm}\right\rangle = -\frac{\hbar^2}{m_e}\langle\Phi_{cw'k}|\langle\Theta_{cw'}|\nabla_e|\Theta_{cw}\rangle\cdot|\nabla_e\Phi_{cwm}\rangle \tag{4.2}$$

For a homonuclear diatomic molecule, the interaction between the ZEKE electron and the molecular ion can be expressed as shown in Eq. (3.11). In Eqs. (4.1) and (4.2) Φ_{cwm} and $\Phi_{cw'k}$ denote the bound state and continuum state of the ZEKE electron, respectively, while Θ_{cw} and $\Theta_{cw'}$ represent the wavefunctions the remaining degrees of freedom of the ion.

Carrying out the time-independent perturbation to the ionic wavefunction, we obtain

$$\langle\Theta_{cw'}|\nabla_e|\Theta_{cw}\rangle = \frac{\left\langle\Theta^0_{cw'}\middle|\nabla_e V'_q\middle|\Theta^0_{cw}\right\rangle}{E^0_{cw}-E^0_{cw'}} \tag{4.3}$$

and

$$\left\langle \Psi_{cw'k}\middle|\widehat{H}'_{IBO}\middle|\Psi_{cwm}\right\rangle = -\frac{\hbar^2}{m_e}\frac{1}{E^0_{cw}-E^0_{cw'}}\left\langle\Phi_{cw'k}\middle|\left\langle\Theta^0_{cw'}\middle|\nabla_e V'_q\middle|\Theta^0_{cw}\right\rangle\cdot\middle|\nabla_e\Phi_{cwm}\right\rangle \tag{4.4}$$

For spherical harmonics, we obtain

$$\left\langle Y_{l'm'}\middle|\frac{\partial Y_{2\bar{m}}}{\partial\theta}\middle|\frac{\partial Y_{lm}}{\partial\theta}\right\rangle + \left\langle Y_{l'm'}\middle|\frac{1}{\sin\theta}\frac{\partial Y_{2\bar{m}}}{\partial\phi}\middle|\frac{1}{\sin\theta}\frac{\partial Y_{lm}}{\partial\phi}\right\rangle = D_{l',l}\langle Y_{l'm'}|Y_{2\bar{m}}|Y_{lm}\rangle \tag{4.5}$$

where

$$\begin{cases} D_{l,l} = 3 \\ D_{l+2,l} = -2l \\ D_{l-2,l} = 2(l+1) \end{cases} \tag{4.6}$$

Therefore, we can obtain the final expression of transition matrix element as

$$\begin{aligned}\left\langle v'^+N'^+JM_J(kl')\middle|\widehat{H}'_{IBO}\middle|v^+N^+JM_J(nl)\right\rangle &= -\frac{\hbar^2}{m_e}\frac{(-e)}{E^0_{v^+N^+}-E^0_{v'^+N'^+}}\langle\chi_{v'^+}|Q(R)|\chi_{v^+}\rangle \\ &\times\left[\frac{4\pi}{5}\sum_{mM^+}\sum_{m'M'^+}\sum_{\bar{m}}C^{JM_J}_{mM^+}C^{JM_J}_{m'M'^+}\langle Y_{l'm'}|Y_{2\bar{m}}|Y_{lm}\rangle\left\langle Y_{N'^+M'^+}\middle|Y^*_{2\bar{m}}\middle|Y_{N^+M^+}\right\rangle\right] \\ &\times\left[D_{l',l}\langle R_{kl'}|r^{-5}|R_{nl}\rangle - 3\langle R_{kl'}|r^{-4}\left|\frac{dR_{nl}}{dr}\right\rangle\right]\end{aligned} \tag{4.7}$$

where $Q(R)$ denotes the core quadrupole moment, χ_{v^+} denotes the wavefunction of vibrational state v^+, and $C^{JM_J}_{mM}$ represents the Clebsch–Gordan coefficient for the coupling between the electronic orbital angular momentum and the core rotational motion; J and M_J denote the total angular momentum and its projection on the space-fixed z axis. Besides, the radial integrals in Eq. (4.7) were performed numerically.

In the case of rotational autoionization of H_2, the numerical results are given in Table 1 for the transition $\{v^+=0,\ N^+=2,\ JM_J(nl)\}\rightarrow\{v'^+=0,\ N'^+=0,\ JM_J(kl)\}$. For a homonuclear molecule like H_2, only transitions $l'=l$ and $l'=l\pm2$ are allowed. In our calculation, the largest contribution comes from the transition $l'=l$, which is few orders of magnitude larger than those from $l'=l\pm2$ mainly due to its larger radial matrix element. Furthermore, from Tables 1 and 2, we can see that the rotational autoionization rates decrease with increasing l and decrease with increasing n for a given l value. From the tables we can see that the n^3 scaling law holds well and gives a very consistent estimation of the autoionization rate. This dependence is easily verified as a result of the factor of $n^{-3/2}$ in the asymptotic bound-state wavefunction with high n.

Table 1
Rotational autoionization for the transition of $\{v^+=0,\ N^+=2,\ JM_J(nl)\}\rightarrow\{v'^+=0,\ N'^+=0,\ JM_J(kl)\}$. The energy of the continuum state is 156 cm^{-1}.

n	l	J	Rate (s^{-1}) IBOA	Rate (s^{-1}) MI
150	2	2	4.076E+07	4.076E+07
150	3	3	4.831E+06	4.830E+06
150	4	4	1.016E+06	1.016E+06
150	5	5	2.940E+05	2.940E+05
150	6	6	1.042E+05	1.042E+05
150	7	7	4.240E+04	4.239E+04
150	8	8	1.900E+04	1.900E+04
150	9	9	9.125E+03	9.124E+03
150	10	10	4.603E+03	4.602E+03
250	2	2	8.805E+06	8.804E+06
250	3	3	1.044E+06	1.043E+06
250	4	4	2.195E+05	2.195E+05
250	5	5	6.356E+04	6.355E+04
250	6	6	2.254E+04	2.254E+04
250	7	7	9.178E+03	9.177E+03
250	8	8	4.118E+03	4.118E+03
250	9	9	1.981E+03	1.981E+03
250	10	10	1.001E+03	1.001E+03

Table 2
Vibrational autoionization for the transition of $\{v^+=1,\ N^+=0,\ JM_J(nl)\}\rightarrow\{v'^+=0,\ N'^+=2,\ JM_J(kl)\}$. The energy of the continuum state is 2035 cm^{-1}.

n	l	J	Rate (s^{-1}) IBOA	Rate (s^{-1}) MI
150	2	2	1.710E+06	1.710E+06
150	3	3	1.906E+05	1.905E+05
150	4	4	3.534E+04	3.534E+04
150	5	5	8.270E+03	8.269E+03
150	6	6	2.135E+03	2.135E+03
150	7	7	5.638E+02	5.637E+02
150	8	8	1.455E+02	1.455E+02
150	9	9	3.569E+01	3.569E+01
150	10	10	8.177E+00	8.178E+00
250	2	2	3.695E+05	3.694E+05
250	3	3	4.117E+04	4.116E+04
250	4	4	7.638E+03	7.637E+03
250	5	5	1.788E+03	1.788E+03
250	6	6	4.621E+02	4.621E+02
250	7	7	1.222E+02	1.222E+02
250	8	8	3.159E+01	3.158E+01
250	9	9	7.765E+00	7.764E+00
250	10	10	1.784E+00	1.786E+00

5. Vibrational autoionization

We consider the vibrational autoionization described by the transition

$$\{v^+=1,\ N^+=0,\ JM_J(nl)\}\rightarrow\{v^+=0,\ N^+=2,\ JM_J(kl)\}$$

The calculated vibrational autoionization rates of H_2 are shown in Table 2. From Table 2, we can see that the behaviors of vibrational autoionization are similar to those of rotational autoionization. With the same rotational transition, the discrepancy between them is mainly attributed to the vibrational matrix elements.

From Tables 1 and 2, we see that the autoionization rates are quite sensitive to n, l. In addition, their energy dependence is given as follows. We have calculated the rates by changing the energy gap and k in Eq. (4.7). For example, for the transitions in Table 1 with $n=150$ and $l=3$, we obtain the rates of 4.842×10^6, 4.757×10^6, $4.647\times10^6\ s^{-1}$ for the energies of 100, 500, 1000 cm^{-1}, respectively. We can see that the variation on rates is

small. In fact, our calculation shows that, in Eq. (4.7), the parenthesis containing the radial matrix element is approximately proportional to the energy difference which is roughly canceled out by the energy gap in the coefficient.

In ZEKE experiments, the influence of Stark-mixing due to the stray residue field needs to be included in our discussion of autoionization rates. Chao et al. have proposed that the optically accessible populations in low-l states would transfer to high-l states, resulting in reduction of core penetration [7]. That is, the low-l states contributing significantly near the ion core experience a stronger interaction with the core. Hence, electrons in low-l states would quickly disappear through various relaxation processes. From Tables 1 and 2, we can see that the transition rate decreases significantly as l increases for both rotational and vibrational autoionization. Consequently, after a long period of delay time, only the states with higher l would survive and be observed in ZEKE experiments. In the case of $l = 3$, the lifetime of rotational autoionization from high Rydberg state is about 1 μs, and that of vibrational autoionization is about one order of magnitude smaller. The autoionization in this range might be observed in the ZEKE experiments with comparable delay time.

6. Discussion

It should be noted that in Section 2 in discussing the theory of ZEKE spectroscopy we calculate the optical absorption rate constant $W_{(av\to cwm)}$ for various transitions like $(av) \to (cwm)$ as a function of laser intensity, pulse-duration, laser-polarization and laser-wavelength. However, in ZEKE spectroscopy, the ZEKE signal is obtained by, in addition to this optical pumping (or absorption), the extraction of ZEKE electrons by a discriminating field and an extraction electric field, and thus the signal can often be interfered by autoionizations. In field extraction of ZEKE electrons, tunneling ionization might play some role.

The rotational and the vibrational autoionization have often been evaluated based on the multipole interaction (MI) model [23–27], which was first pointed out by Russek et al. [23] and followed by Jungen and Miescher [24] and Eyler [25]. For example, for the Fermi golden rule expression of autoionization $cwm \to cw'k$ due to V'_q the rate can be expressed as

$$W_{(cwm\to cw'k)} = \frac{2\pi}{\hbar}\left|\left\langle \Psi_{cw'k}\middle|V'_q\middle|\Psi_{cwm}\right\rangle\right|^2 \rho(E_k) \tag{6.1}$$

It follows that

$$\begin{aligned}&\left\langle v'^+N'^+JM_J(kl')\middle|V'_q\middle|v^+N^+JM_J(nl)\right\rangle \\ &= -e\langle\chi_{v'^+}|Q(R)|\chi_{v^+}\rangle\langle R_{kl'}|r^{-3}|R_{nl}\rangle \\ &\quad\times\left[\frac{4\pi}{5}\sum_{mM^+}\sum_{m'M'^+}\sum_{\bar m} C^{JM_J}_{mM^+}C^{JM_J}_{m'M'^+}\langle Y_{l'm'}|Y_{2\bar m}|Y_{lm}\rangle\left\langle Y_{N'^+M'^+}\middle|Y^*_{2\bar m}\middle|Y_{N^+M^+}\right\rangle\right]\end{aligned} \tag{6.2}$$

Numerical calculations have been performed to compare the above expression with ours based on the use of IBOA. The results are given in Tables 1 and 2 denoted as MI. We can see that the agreement for both vibrational and rotational autoionization rates is excellent. Next, we shall compare the formulations between the two models as discussed by Russek et al. [23].

Referring to Eqs. (2.7) and (2.8), we can obtain the unperturbed Hamiltonian by neglecting the higher order interactions:

$$\hat H^0_{ion}\Theta^0_{cw} = U^0_{cw}\Theta^0_{cw} \tag{6.3}$$

$$\left(\hat T_e - \frac{e^2}{r}\right)\Phi^0_m = E^0_m\Phi^0_m \tag{6.4}$$

We note that to the zeroth-order, this representation is the same as the traditional Hund's case (d). From Eq. (6.4), we can derive that

$$\left\langle\Phi^0_f\middle|V'_q\middle|\hat T_e\Phi^0_i\right\rangle - \left\langle\hat T_e\Phi^0_f\middle|V'_q\middle|\Phi^0_i\right\rangle = \left(E^0_i - E^0_f\right)\left\langle\Phi^0_f\middle|V'_q\middle|\Phi^0_i\right\rangle \tag{6.5}$$

Also notice that

$$\begin{aligned}&-\frac{\hbar^2}{2m_e}\left\langle\nabla^2_e\Phi^0_f\middle|V'_q\middle|\Phi^0_i\right\rangle \\ &= -\frac{\hbar^2}{2m_e}\left[\left\langle\Phi^0_f\middle|V'_q\middle|\nabla^2_e\Phi^0_i\right\rangle + 2\left\langle\Phi^0_f\middle|\nabla_eV'_q\cdot\middle|\nabla_e\Phi^0_i\right\rangle + \left\langle\Phi^0_f\middle|\nabla^2_eV'_q\middle|\Phi^0_i\right\rangle\right]\end{aligned} \tag{6.6}$$

To derive Eq. (6.6), we need to perform integration by parts two times to pass ∇_e to the right side. Substituting Eq. (6.6) to Eq. (6.5), we obtain

$$\begin{aligned}\left\langle\Phi^0_f\middle|V'_q\middle|\Phi^0_i\right\rangle = &-\frac{\hbar^2}{2m_e}\frac{1}{\left(E^0_f - E^0_i\right)} \\ &\times\left[2\left\langle\Phi^0_f\middle|\nabla_eV'_q\cdot\middle|\nabla_e\Phi^0_i\right\rangle + \left\langle\Phi^0_f\middle|\nabla^2_eV'_q\middle|\Phi^0_i\right\rangle\right]\end{aligned} \tag{6.7}$$

Because the quadrupole interaction involves the core dependence, we shall multiply both sides of Eq. (6.7) by the ionic wavefunctions and integrate over the ionic coordinates. Then, we obtain the autoionization matrix element used in the MI model

$$\begin{aligned}\left\langle\Theta^0_{cw'}\middle|\left\langle\Phi^0_f\middle|V'_q\middle|\Phi^0_i\right\rangle\middle|\Theta^0_{cw}\right\rangle = &-\frac{\hbar^2}{2m_e}\frac{1}{\left(E^0_f - E^0_i\right)} \\ &\times\left[2\left\langle\Theta^0_{cw'}\middle|\left\langle\Phi^0_f\middle|\nabla_eV'_q\cdot\middle|\nabla_e\Phi^0_i\right\rangle\middle|\Theta^0_{cw}\right\rangle\right. \\ &+\left.\left\langle\Theta^0_{cw'}\middle|\left\langle\Phi^0_f\middle|\nabla^2_eV'_q\middle|\Phi^0_i\right\rangle\middle|\Theta^0_{cw}\right\rangle\right]\end{aligned} \tag{6.8}$$

Switching the sequence of the two integrals, the first term on the right-hand side is in accordance with the matrix element in Eq. (4.2) in the formulation of IBOA, while the second term is evidently zero for the quadrupole term is a solution of Laplace equation in the electronic coordinate. Here we shall stress that this derivation is based on the use of multipole expansion, in which we employed the unperturbed wavefunction and its first-order correction. The generality of Eq. (6.8) should be examined for other assumptions and conditions. In fact, the origins of the two formulations (Eqs. (4.2) and (6.1)) are quite different and the results are not necessarily equivalent. At any rate, we see that the IBOA approach is more versatile and can be systematically generalized to include other higher order interactions. As emphasized previously [23,25], the present model works mainly for non-penetrating states. For penetrating states, higher order terms need to be included.

It is also interesting to compare our IBOA to the MQDT [3,4,9–11], which has been employed to study high Rydberg states. The MQDT is a scattering theory while our IBOA is based on eigenfunction expansion; i.e., a bound state description. Using the IBOA, the interactions between the Rydberg electron and the ion core can be systematically included and calculated. Therefore, the IBOA in this sense is useful in providing an alternative approach to the MQDT to better understand the many faces of high Rydberg states.

Acknowledgements

This work has been supported by National Science Council of ROC and Academia Sinica. The works of Yi-Hsieh Wang and S.D. Chao are also partly supported by the CQSE National Taiwan University through 97R0066-66.

References

[1] K. Müller-Dethlefs, M. Sander, E.W. Schlag, Chem. Phys. Lett. 112 (1984) 291.
[2] E.W. Schlag, ZEKE Spectroscopy, Cambridge University Press, Cambridge, 1998.

[3] F. Merkt, T.P. Softley, Int. Rev. Phys. Chem. 12 (1993) 205.
[4] S.T. Pratt, Annu. Rev. Phys. Chem. 56 (2005) 281.
[5] S.D. Chao, H.L. Selzle, H.J. Neusser, E.W. Schlag, L. Yao, S.H. Lin, Z. Phys. Chem. 221 (2007) 633.
[6] S.D. Chao, S.H. Lin, H.L. Selzle, H.J. Neusser, E.W. Schlag, Trend Appl. Spectrosc. 7 (2009) 1.
[7] S.D. Chao, M. Hayashi, S.H. Lin, E.W. Schlag, J. Chin. Chem. Soc. 45 (1998) 491.
[8] F. Remacle, R.D. Levine, Int. J. Quant. Chem. 67 (1998) 85.
[9] S. Fredin, D. Gauyacq, M. Horani, Ch. Jungen, G. Lefevre, F. Masnou-Seeuws, Mol. Phys. 60 (1987) 825.
[10] F. Merkt, T.P. Softley, Phys. Rev. A 46 (1992) 302.
[11] A. Kirrander, H.H. Fielding, Ch. Jungen, J. Chem. Phys. 127 (2007) 164301.
[12] J. Xie, R.N. Zare, J. Chem. Phys. 93 (1990) 3033.
[13] J. Xie, R.N. Zare, J. Chem. Phys. 97 (1992) 2891.
[14] A.D. Buckingham, B.J. Orr, J.M. Sichel, Philos. Trans. R. Soc. Lond. A 268 (1970) 147.
[15] J.M. Sichel, Mol. Phys. 18 (1970) 95.
[16] M.S. Ford, K. Müller-Dethlefs, Phys. Chem. Chem. Phys. 6 (2004) 23.
[17] M.S. Ford, R. Lindner, K. Müller-Dethlefs, Mol. Phys. 101 (2003) 705.
[18] S.H. Lin, J. Chem. Phys. 44 (1966) 3759.
[19] R.S. Berry, J. Chem. Phys. 45 (1966) 1128.
[20] F. Merkt, P.M. Guyon, J. Chem. Phys. 99 (1993) 3400.
[21] F. Merkt, T.P. Softley, J. Chem. Phys. 96 (1992) 4149.
[22] T.P. Softley, A.J. Hudson, J. Chem. Phys. 101 (1994) 923.
[23] A. Russek, M.R. Patterson, R.L. Backer, Phys. Rev. 167 (1968) 17.
[24] Ch. Jungen, E. Miescher, Can. J. Phys. 47 (1969) 1769.
[25] E.E. Eyler, Phys. Rev. A 34 (1986) 2881.
[26] C.R. Mahon, G.R. Janik, T.F. Gallagher, Phys. Rev. A 41 (1990) 3746.
[27] R.D. Gilbert, M.S. Child, Chem. Phys. Lett. 287 (1991) 153.